Published in final edited form as:
Bone. 2011 May 1; 48(5): 1095–1102. doi:10.1016/j.bone.2011.01.002.

Mitigation of Bone Loss with Ultrasound Induced Dynamic Mechanical Signals in an OVX Induced Rat Model of Osteopenia

Suzanne L. Ferreri[1], **Roger Talish**[2], **Titi Trandafir**[2], and **Yi-Xian Qin**[1,*]

Suzanne L. Ferreri: suzanne.ferreri@gmail.com; Roger Talish: rjt@talish.com; Titi Trandafir: TTrandafir@juvent.com; Yi-Xian Qin: Yi-Xian.Qin@sunysb.edu

[1] Orthopaedic Bioengineering Research Lab, Department of Biomedical Engineering, Stony Brook University, Stony Brook, New York 11794

[2] Juvent, Inc., Sommerset, NJ 08873

Abstract

This study tests the hypothesis that an ultrasound generated dynamic mechanical signal can attenuate bone loss in an estrogen deficient model of osteopenia. Eighty-four, sixteen week old Sprague-Dawley rats were divided into six groups: baseline control, age-matched control, ovariectomy (OVX) OVX control, OVX + 5 mW/cm^2 ultrasound (US), OVX + 30 mW/cm^2 US and OVX + 100 mW/cm^2 US. Low intensity pulsed ultrasound (LIPUS) was delivered transdermally at the L4/L5 vertebrae, using gelcoupled plane wave US transducers. The signal, characterized by 200μs pulses of 1.5 MHz sine waves repeating at 1 kHz with spatial-averaged temporal-averaged (SATA) intensities of 5, 30 or 100mW/cm^2, was applied 20 min/day, 5 days/week for 4 weeks. OVX treatment reduced bone volume fraction 40% and compromised microstructure at 4 weeks. LIPUS treatment, however, significantly increased BV/TV 33% compared to OVX controls for the 100mW/cm^2 treated group. SMI, and Tb.N showed significant improvements compared with OVX for the 100mW/cm^2 treated group and Tb.Th was significantly improved in the 30 and 100mW/cm^2 treated groups. Improvements in bone's microstructural characteristics with 100mW/cm^2 US treatment translated into improved load bearing characteristics, including a significant, 42% increase in apparent level Elastic Modulus compared to OVX controls. Significant improvement of trabecular mechanical strength is also observed in the treated animals, e.g., principal compressive stress (represent bone's ability to resist loads) was significantly higher compared to OVX controls. Histomorphometric analysis also showed that treatment with 100mW/cm^2 US resulted in a 76% improvement in MS/BS. In addition, measures of bone quantity and quality at the femoral metaphysis suggest that LIPUS is site specific. This study indicates that ultrasound, delivered at specific intensities, has beneficial effects on intact bone and may represent a novel intervention for bone loss.

Keywords

Therapeutic Ultrasound; bone remodeling; mechanotransduction; low intensity ultrasound; Ovariectomy

[*]Corresponding author: Yi-Xian Qin, Ph.D., Department of Biomedical Engineering, Stony Brook University, Bioengineering Building, Rm 215, Stony Brook, NY 11794-5281, Yi-Xian.Qin@sunysb.edu.

Introduction

Osteoporosis is a disease characterized by decreased bone mass and progressive erosion of the microstructure. As a result, key skeletal sites such as the hip, spine and wrist are at increased risk of fracture in response to minimal trauma. Current treatments include hormonal, pharmacologic and mechanical strain interventions. Hormonal and pharmacologic interventions are often associated with adverse side effects and target the skeleton as a whole, as opposed to specifically targeting skeletal sites at increased risk for failure. Mechanical strain interventions, however, are noninvasive and have demonstrated promising results. In vivo studies have shown low-magnitude, high- frequency vibrations to be anabolic in both human[1] and animal models [2]. In addition, whole bone accelerations have been shown to be anabolic to bone [3,4]. A contributing mechanism by which low-magnitude mechanical stimulations act, could involve bone fluid flow. Previous studies have shown that in the absence of mechanical strain, intramedullary bone fluid flow can drive bone remodeling [5,6].

It has been suggested that in bone, ultrasound behaves as a mechanical wave, generating local pressure gradients. This may result in the production of anabolic shear forces on cell membranes or changes in local solute concentrations [7,8]. These gradients could drive local fluid flow, potentially resulting in an anabolic signal. Therefore, low intensity pulsed ultrasound (LIPUS) may offer a noninvasive method for delivery of high frequency, low amplitude and large cycle number, dynamic mechanical signals.

In vitro studies have shown that LIPUS is capable of increasing osteoblast proliferation and stimulating endochondral ossification in excised tissues [9–12]. It has also been shown that ultrasound signal intensity plays an important role in modulating the response of osteoblasts in vitro [13,14]. One potential mechanism by which ultrasound acts could involve integrin receptors. An in vitro study has shown that osteoblasts up-regulate inducible nitric-oxide synthase (iNOS) via an integrin receptor in osteoblasts [15]. In addition, ultrasound may act to increase bone morphogenetic protein-2 (BMP-2) [16]. In vivo studies have also shown that LIPUS accelerated fracture healing in both animal [17–21] and human models [22–25]. In addition, Yang et al. showed that bone's response to ultrasound during fracture healing was sensitive to ultrasound signal intensity [21]. While LIPUS has demonstrated effects on regulating osteoblastic activities in vitro and promote fracture healing in vivo, one may assume that ultrasound may play a role in modulating osteopenia associated with estrogen deficiency and aging as well. However, there is limited, conflicting evidence with respect to the effectiveness of LIPUS in treating non-fracture related bone diseases in vivo [26–30]. In one study, 26 week old rats (~332g) were overectomized and LIPUS (30mW/cm^2, 1 MHz pulsed at 1kHz, 20min/day, 6 days/week, for 12 weeks) was delivered to the proximal tibia. This study found that US signals had no effect on wet weight or bone formation rate (BFR) [27]. Another study evaluated the effects of LIPUS (30mW/cm^2, 1.5MHz pulsed at 1kHz, 20min/day,for 20 days) at the proximal femur of 200g female Holstman rats subjected to 30 days OVX prior to treatment. Histological analysis using mason tricrome staining showed qualitative improvements in ultrasound treated animals not observed in control groups [29]. In a more recent study, LIPUS (1.5 MHz, 1.0 kHz pulse repetition, 30 mW/cm^2, with intensity of 200μs pulse length) was applied to 14-week-old OVX mice for 6-week; and indicated that bone volume of treated limb was significantly enhanced compared to the contralateral control [38]. In light of the differences among US stimulation protocols used in these studies, it is remained unclear what role ultrasound signal parameters, in particular signal intensity, play in bone's response.

The objective of this study was to explore the therapeutic potential of LIPUS for treatment of bone loss associated with estrogen deficient osteopenia using high resolution three-

dimensional imaging and computational structural analysis techniques. This study tests the hypothesis that an ultrasound generated dynamic mechanical signal can mediate bone loss and changes to structural integrity in an estrogen deficient model of osteopenia. To this end, we have completed a study in which we tested the effectiveness of various US signal intensities in preserving bone's micro architecture and mechanical integrity using high resolution imaging, dynamic histomorphometry and computer modeling techniques.

Materials and Methods

Experimental Design

All surgical and therapeutic procedures were approved by the Institutional Animal Care and Use Committee (IACUC) at Stony Brook University. Sixteen week old, virgin female, Sprague-Dawley rats (304 ± 9g) were obtained from Charles River Laboratories (Wilmington, MA) and subjected to either ovariectomy (OVX) or sham operation. Animals were allowed to recover for 3 days, after which they were randomly assigned to one of six groups: (1) baseline control (n=18), (2) age-matched (sham-operated) control (n=21), (3) OVX control(n=20), (4) OVX + 5 mW/cm^2 ultrasound stimulation (US) (n=8), (5) OVX + 30 mW/cm^2 US (n=8) and (6) OVX + 100 mW/cm^2 US (n=8). The lower animal number in the stimulated group was due to the availability of ultrasound delivery devices. All animals were housed individually in standard cages at 24°C and allowed free access to standard rodent chow and tap water. Body weight and food consumption were recorded at day zero and monitored bi-weekly throughout the study. Upon completion of the study, animals were euthanized via CO_2 asphyxiation.

US Treatment

Under isofluorane anesthesia, animals were positioned in sternal recumbency on a custom platform and therapeutic ultrasound was delivered transdermally over the posterior aspect of lumbar vertebra L4 and L5 using a 1 inch diameter disk plane wave ultrasound transducer (manufactured by Piezo Technologies and mounted on an Ultrasonic Instrument delivered by Juvent Medical Inc). To maximize coupling of the transducer with the skin surface, fur was removed from the lumbar spine region and an ultrasonic coupling gel (Aquasonic, Inc.) was applied between the skin and ultrasound transducer. The signal was characterized by 200μs pulses of 1.5 MHz sine waves with a PRF (Pulse Repetition Frequency) of 1 kHz and spatial-averaged temporal-averaged intensity (I_{SATA}) equal to 5, 30 or 100 mW/cm_2. Treatment was applied 20 min/day, 5 days/week for 4 weeks. Ultrasound signals were calibrated at the beginning, midpoint and end of the study using a membrane hydrophone (Precision Acoustics, Ltd., UK). To minimize potential confounding effects due to isofluorane exposure, age-matched control and OVX control animals were simultaneously subjected to 20 minutes of isofluorane anesthesia per day, 5 days/week for 4 weeks. Upon completion of the study, animals were sacrificed via CO_2 asphyxiation and the L5 vertebra was removed to evaluate the effects of localized ultrasound treatment and the left femur was removed to quantify systemic effects in the skeleton away from the treatment site. Samples were then cleaned of soft tissue and stored in saline soaked gauze at −40°C.

Microcomputed tomography

The L5 vertebra and left femur were imaged at 15μm isotropic resolution using μCT (μCT40, SCANCO) with energy (E) and intensity (I) equal to 55 kVp and 145 μA respectively. Cancellous bone was then manually segmented from a 1.5mm long axial ROI from the cranial third of the anterior vertebral body and a 1.5mm long region of the femoral metaphysis (Figure 2). Cancellous microstructure was then characterized using standardized techniques to determine bone volume fraction (BV/TV), structural model index (SMI),

connectivity density (Conn.D.), trabecular number (Tb.N.), trabecular thickness (Tb.Th.) and trabecular spacing (Tb.Sp.).

Finite Element Analysis

Three-dimensional image data from the L5 vertebra was used to generate specimen specific finite-element models, which were then used to evaluate the load bearing capabilities for each sample. Voxel based finite element meshes were created using custom software based on the pixel-to-voxel technique, in which each pixel is represented by an eight-noded cuboid element. Disassociated regions of the model, which did not intersect virtual-cut plane surfaces, were removed to ensure convergence. In each case this step removed less than 0.1% of the total bone volume fraction. Trabecular tissue was assumed to behave as a homogenous, linear elastic isotropic solid (E=18GPa & v=0.3) and full friction boundary conditions were assigned at the superior and inferior surfaces. Trabecular samples were subjected to 0.5% compressive strain in the cranio-caudal direction and solved using a commercial, nonlinear finite element solver (ABAQUS v6.4, Dassault Systemes, Inc., Providence, RI). The apparent elastic modulus, which reflects the mechanical contributions of bone material and microstructural organization, was calculated as the ratio of the total applied force at 0.5% strain to the area of the sample encompassed by the CT contour lines. The average and coefficient of variation (COV) of *von* Mises stress are calculated. *von* Mises stress may be used as a measure of local tissue failure and an increase in the variability among *von* Mises stresses could indicate an increased propensity for local stress concentrations which could lead to local tissue failure [31]. The average and 75^{th} percentile of maximum principal stress among all elements in the model describe the average and peak stress values experienced by elements throughout the trabecular sample. The average and 75^{th} percentile of strain energy density (SED) were also calculated at each element in the model and describe the concentration of strain energy in individual elements throughout the model. In trabecular bone, increased SED has been correlated with sites of local bone remodeling and may indicate the potential for a mechanically based bone remodeling signal [32].

Histological Analysis

Intraperitoneal Calcein injections (10 mg/kg) were made two and 16 days prior to the end of the study. Following μCT scanning, a 3mm thick transverse slice from the upper third of the L5 vertebra was cleaned and embedded in a low viscosity epoxy resin (EpoThin, Buhler, Inc.). A 1mm slice was then cut using a diamond wire saw and polished to a thickness of ~75 μm. The commercial system Osteomeasure (OsteoMetrics Inc, Decatur, GA) was used to make histomorphometric measurements by tracing calcein labels in the trabecular bone. Histomorphometric bone volume fraction (BV/TV — Histo, %), mineralizing surface/bone surface (MS/BS, %), mineral apposition rate (MAR, μm/day), and bone formation rate (BFR/BS, $\mu m^3/\mu m^2/yr$) are reported [33].

Data Analysis

All values are reported as mean ± standard deviation, unless noted otherwise. One-way analysis of variance (ANOVA) and Tukey's post-hoc test was used to detect differences between groups for body weight, food consumption, morphological indices and mechanical strength parameters. Significance was determined at $p \leq 0.05$ and $p \leq 0.001$. Correlations between signal intensity and either microstructural parameters or mechanical strength parameters were determined using multiple linear regressions and Pearson's product moment correlation coefficient. All statistical analyses were performed using SigmaStat v3.5 (Systat Software, Inc., San Jose, CA, USA).

Results

Body Mass and Food Intake

At day zero, there were no significant differences in body mass among any of the experimental groups (Figure 1). Body mass for age-matched controls did not vary significantly from baseline throughout the duration of the 28 day study. Body mass for OVX and OVX + LIPUS treated groups, however, increased significantly throughout the study (17%, $P<0.001$) compared to age-matched controls. No differences in body mass were observed among OVX control and OVX + LIPUS treated groups. Increased body weight was not associated with increased food consumption, which remained constant for all groups throughout the study.

OVX effects on bone microarchitecture and mechanical integrity

At 28 days post-surgery, OVX treatment was associated with substantial alterations in cancellous bone volume and morphology (Table 1 & Figure 3). OVX controls had 40% lower ($p<0.01$) BV/TV than Age-matched controls. Tb.N. decreased 17% ($p<0.001$), Tb.Th. decreased 19% ($p<0.001$) and Tb.Sp. increased 24% ($p<0.001$). OVX was also associated with higher SMI (436%, $p<0.001$) compared to age-matched controls. No changes, however, in Conn.D. were observed in OVX treated animals.

Bone's load bearing characteristics were also strongly affected by OVX (Table 2 & Figure 4). At the apparent level, Elastic Modulus was 51% lower ($p<0.001$) for OVX treated animals compared to age matched controls. Changes were also observed in average tissue stresses. Mean *von* Mises stress was 24% lower ($p<0.001$) while the *von* Mises stress coefficient of variation was 21% higher ($p<0.001$). Additionally, the mean and 75^{th} percentile of maximum principal stress was 23 and 45% lower respectively ($p<0.001$). Strain energy density, an indicator of local tissue fatigue and failure, had lower mean and 75^{th} percentile values (26% $p<0.001$ and 32% $p<0.001$) compared to age-matched controls.

Effect of age on microarchitecture and mechanical integrity

Comparisons between age-matched and baseline controls were used to address potential changes in bone microarchitecture due to rodent maturation over the course of the experiment. No significant differences were identified among any of the morphological or mechanical strength parameters examined in this study.

Effects of therapeutic ultrasound treatment on microarchitecture

The effects of therapeutic ultrasound on bone microarchitecture from the L5 vertebra are shown in Figure 3 and Table 1. BV/TV was positively correlated ($R^2=0.96$) with ultrasound signal intensity, and was significantly higher (33%, $p<0.001$) in the 100mW/cm^2 US treated group compared to OVX controls. In addition, BV/TV was also 23% higher in the 100mW/cm^2 treated group compared to that of the 5mW/cm^2 treated group. However, when compared with age-matched controls, BV/TV was significantly lower in all US treated groups. Similarly, SMI was 48% lower ($p<0.001$) in the 100mW/cm^2 US treated group compared to OVX controls, and was negatively correlated ($R^2= 0.99$) to intensity. When compared to age matched controls, SMI was significantly higher in each of the US treated groups. There was no difference in Conn.D. between OVX and age-matched controls, and no differences between US treated groups and either OVX or age-matched controls.

Tb.Th. was significantly higher in the 30mW/cm^2 and 100mW/cm^2 treated groups compared to OVX controls (11%, $p<0.05$ and 13%, $p<0.001$) and had strong correlation to signal intensity ($R^2 = 0.71$). Compared to Age-matched controls, Tb.Th. was significantly lower in each of the US treated groups. Tb.N. was positively correlated to signal intensity ($R^2 = 0.97$)

and was significantly higher (12%, $p<0.05$) in the 100mW/cm^2 treated group. Compared with age matched controls, Tb.N. was significantly lower for the 5 and 30mW/cm^2 signals (−15%, $P<0.001$ and −11%, $p<0.05$), however there was no significant difference in Tb.N. between age-matched controls and the 100mW/cm^2 treated group. Tb.Sp. also showed a strong negative correlation with signal intensity ($R^2 = 0.94$) and was significantly lower (−14%, $P<0.001$) for the 100mW/cm^2 treated group compared to OVX controls. Compared with age matched controls, Tb.Sp. was significantly higher for the 5 and 30mW/cm^2 signals (21%, $P<0.001$ and 15%, $p<0.05$), however there was no significant difference in Tb.N. between age-matched controls and the 100mW/cm^2 treated group.

Effects of therapeutic ultrasound treatment on mechanical integrity

The effects of therapeutic ultrasound on bone's mechanical integrity at the L5 vertebra are shown in Figure 4 and Table 2. Similar trends were also observed in bone's response to mechanical strain. At the apparent level, Elastic Modulus was positively correlated with US signal intensity ($R^2 = 0.95$), and was significantly higher for the 100mW/cm^2 US treated groups (42%, $p<0.05$) compared to OVX controls. However, compared to age-matched controls, each of the US treated groups had a significantly lower Elastic Modulus. Mean *von* Mises stress and the coefficient of variation of *von* Mises stress were strongly correlated with ultrasound signal intensity ($R^2 = 0.99$ and $R^2 = 0.99$), but were not significantly different compared to OVX controls. When compared to age-matched controls, both mean *von* Mises stress and the coefficient of variation of *von* Mises stress were significantly different for the 5 and 30mW/cm^2 US treated groups, however, there were no significant differences between age-matched controls and 100mW/cm^2 US treated groups.

Positive correlations were also observed between mean maximum principal stress and the 75th percentile of maximum principal stress and US signal intensity ($R^2 = 0.99$ and $R^2 = 0.99$). While there were no significant differences between mean maximum principal stress and OVX controls, the 75th percentile of maximum principal stress was significantly higher in the 100mW/cm^2 US treated groups and OVX controls. Both mean maximum principal stress and the 75th percentile of maximum principal stress were significantly different compared with age-matched controls.

Lastly, we considered strain energy distributions in US treated groups compared to OVX and age-matched controls. Both average and 75th percentile of strain energy densities were well correlated with US signal intensity, but were not significantly different compared to OVX controls. When compared with age-matched controls, the 5 and 30mW/cm^2 US treated groups were significantly different, but there were no differences between the 100mW/cm^2 US treated group and age-matched controls.

Bone Morphology at a Non-stimulated Skeletal Site

Following four weeks of OVX, animals had 66% ($P<0.001$) lower BV/TV at the femoral metaphysis compared to age matched controls. In addition, Conn.D. decreased 66% ($P<0.001$), SMI decreased 407% ($P<0.001$), Tb.N. decreased 52% ($P<0.001$), Tb.Th. decreased 28% ($P<0.001$) and Tb.Sp. increased 123% ($P<0.001$). However, there were no significant differences between any of the US treated groups when compared with OVX controls.

Effects of US treatment on static and dynamic histomorphometry

The results of histomorphometric analysis are reported in Table 3. Trabecular BV/TV measured by 2D histomorphometry showed a significant decrease following 28 days OVX (56%, $p<0.001$) (Figure 5). Treatment with 100mW/cm^2 LIPUS significantly increased BV/TV compared to OVX controls (80%, $p<0.001$); however BV/TV values for this group were

still significantly lower than age-matched controls (−21%, $p<0.001$). Following OVX, significant decreases were found in MS/BS (−50%, $p<0.001$), MAR (−23%, $p<0.001$) and BFR/BS (−52%, $p<0.001$). There was no significant improvement in MAR or BFR/BS for any of the groups treated with LIPUS. However, treatment with 100mW/cm^2 US showed a 76% ($p<0.05$) improvement in MS/BS.

Discussion

In this study, LIPUS was proposed as a therapeutic intervention for treatment of bone loss based on its effectiveness in previous in vitro and in vivo fracture related studies as well as its potential as an anabolic high frequency mechanical signal. Our data indicate that low intensity pulsed ultrasound signals, were able to partially mitigate detrimental changes to bone morphology and mechanical robustness induced by estrogen deficiency. Furthermore, we have also shown that bone's response is strongly correlated with ultrasound signal intensity. Here, at 28 days post-OVX, vertebral trabecular bone had lower BV/TV, decreased Tb.Th. and Tb.N., Tb.Sp., MS/BS, MAR and BFR/BS. Apparent modulus as well as tissue level stress and strains were also compromised. US treatment, however, was in part capable of mitigating the effects, as was shown by significant improvements over OVX controls and in some cases returning values to a level similar to that of the age-matched controls.

Our study also found that adaptations were not observed at a remote skeletal site, indicating that bone's response to US was site specific. This aspect of our signal may offer a unique advantage in the treatment of post-menopausal bone loss. While post menopausal osteoporosis causes systemic changes to the skeleton, fractures are typically localized to key skeletal sites such as the hip, wrist and spine. For this reason it may be particularly advantageous to treat those sites, which pose significant risk, while minimizing the potential for unwanted side effects.

This study addresses the effects of three different spatial-averaged temporal-averaged ultrasound signal intensities: 5mW/cm^2, 30mW/cm^2 and 100mW/cm^2. These signals represent the low, moderate and higher ranges of what is typically considered low-intensity ultrasound. Ultrasound signals have been shown to be highly effective in stimulating delayed and nonunion fractures in animal models at 11mW/cm^2 [34], 30mW/cm^2 [17,18] and 100mW/cm^2 [21]. Finally, one concern for the development of any medical ultrasound device is that of thermal heating. At very high intensities, > 1000mW/cm^2, it is possible to generate changes in local tissue temperature > 1°C, which would exceed established safety limits [35]. Several studies have shown that intensities as high as 50mW/cm^2 did not induce changes in temperature > 1°C [36,37]. As close to the 50mW/cm^2 range and far below the 1000mW/cm^2 range, the 100mW/cm^2 signals used in this study are below intensities known to induce thermal heating and are believed to be safe for treatment in humans and animals.

While caution must be used in extrapolating these results to humans, the results of this study suggest that LIPUS may serve as an effective intervention or a complimentary treatment for estrogen deficient bone loss. The effectiveness of LIPUS in treating delayed and nonunion fractures has been widely established in controlled studies involving both human [22–25] and animal models [17–21]. However, this application presents a unique environment dominated by acute inflammation and altered bone geometry. Subsequently, there is conflicting evidence regarding the use of therapeutic US in intact bone. In a similar study, Carvalho et al. noted a qualitative increase in new bone formation in the cancellous region of the proximal femur when exposed to 30mW/cm^2 LIPUS treatment [29]. While our study did not find significant improvements in BV/TV with 30mW/cm^2 US intervention, we observed a significant improvement with 100mW/cm^2. Our study also supports the findings

of Lim et al., who showed that low-intensity US stimulation was capable of preventing bone loss in your adult OVC mice [38].

Our findings are in discord with a previous study by Warden et al., which found that LIPUS was ineffective in preserving bone mineral density (BMD) and BV/TV [27]. In contrast, our study noted significant improvements in cancellous bone microstructure and subsequent improvements in structural integrity. One possible explanation for this difference could involve the confounding results of slight growth due to animal age. In our study animals were 4 and 5 months old at the start and end of the study while in the Warden et al. study animals were 6.5 and 9.5 months old respectively. In addition, differences could arise due to the targeted skeletal site. Our study addressed the effects of treatment at the lumbar spine, while the Warden et al. study targeted the proximal tibia and distal femur. Additional explanation may include the higher LIPUS dosage used in this study. Ultrasound has also been tested in other murine models of bone remodeling under various treatments. Yang et. al. found that a 125mW/cm^2 US was ineffective in preserving BMD and BV/TV in rats following sciatic nervectomy [39]. Similarly, Spadaro et al, found no differences in BMD at the femur/tibia between treated and untreated four week old rats [30].

The results of the current study indicate that LIPUS was capable of increasing MS/BS relative to untreated OVX controls. While this improvement was found to be significant, the results do not completely explain the improvements in bone morphology following US treatment. Therefore, it is possible that US acts to both improve bone formation and reduce bone resorption. One limitation of the current study is that we did not measure the effects of bone resorption using tartrate-resistant acid phosphatase (TRAP) staining. In the current study, our preparation of samples precludes this type of analysis. However, future studies will be sure to incorporate this crucial assay.

While the precise mechanism by which LIPUS acts in bone remains unclear, several possibilities have been suggested. First, ultrasound may act to generate an electric field, which could then drive an osteogenic adaptation [40]. While we did not specifically address this issue in our study, an in vitro study has shown that ultrasound could generate an electric field in the range believed to be anabolic to bone tissue [41]. A second potential mechanism could involve thermal heating. However, given the maximum range of intensities addressed in this study, it is unlikely that heating plays a role in bone's response [42,43]. Ultrasound has also been shown to induce stable cavitation [44], however, given the intensities used in our study, this is highly unlikely. Lastly, it has been suggested that acoustic streaming may play a role in bone's response. Because ultrasound behaves as a mechanical wave in bone, it may be possible to generate local pressure gradients within bone's microporosities [7,8]. Several recent studies have suggested that fluid movement within these structures could generate the mechanical signals associated with an increased osteogenic response [45,46].

It is important to recognize that ultrasound signal attenuation likely plays an important role in the delivery of US energy[47]. It has been estimated that, ignoring attenuation, an US signal with a spatial-averaged temporal-averaged intensity of 30mW/cm^2 exerts a spatial-averaged temporal-averaged force in the vicinity of 2mg/cm^2 [28]. This force is far below physiologic loads or high frequency strain signals, which have been shown to be anabolic. This suggests that acoustic radiation force plays an insignificant role in bone's response to the LIPUS signals addressed in this study.

Several limitations should be considered when interpreting the results of this study. First, in our study ultrasound treatment was introduced immediately following OVX. However, in a clinical setting treatment is typically introduced after substantial bone loss has occurred. Future studies will address this important aspect. In addition our study is limited in that it

depicts a single time point in the time course of ultrasound treatment. Future studies will take advantage of in vivo microCT imaging technology, which will allow for the measurement of changes to bone's microarchitecture throughout treatment. Another limitation is that we do not know precisely how the ultrasound wave propagates through the skin, fat, muscle and bone to act at the cancellous region addressed in this study. Given our current technologies, it would be extremely difficult to gain reliable in vivo measurements of signal transmission. However, we have conducted ex vivo measurements using a hydrophone, which suggest that approximately 30% of the initial ultrasound signal penetrates through the skin, muscle and cortical shell. Furthermore, ongoing studies in our lab will continue to develop computer models which simulate acoustic wave propagation through realistic tissue geometries. Such studies will help to explain the local environment during ultrasound stimulation. Finally, the histomorphometry analysis indicated that bone formation/turnover in OVX were lower than in age-matched controls. One would expect that after only 28 days of ultrasound treatment these value would be higher than control as estrogen-deficiency may accelerate turnover, even though a net bone loss may occur. Logically, further study should have included the analyses in both bone formation and resorption. While OVX treatment may increase bone turnover, it will ultimately lead to net bone loss, in which the resorption may suppress the turnover.

In summary, we have shown that LIPUS is capable of partially mitigating the adverse changes to bone induced by estrogen deficient osteopenia and that bone's response is sensitive to US signal intensity. To date, there is conflicting evidence for US as a treatment in intact bone; therefore, future studies will need to address the effects of US signal parameters (frequency, pulse duration, intensity and modulation). In addition, the mechanisms by which US acts to deliver an anabolic signal in bone remain elusive, indicating the need for further in vitro and computer simulation studies. It is interesting to note that recent developments in qualitative ultrasound (QUS) technology have shown that broadband ultrasound attenuation (BUA) is sensitive not only to bone quantity, but to measures of bone quality as well [48]. This suggests that US technology could be capable of integrating prophylaxis, treatment and diagnostic applications.

Acknowledgments

This work is kindly supported by NIH (AR49286 and AR52379), National Space Biomedical Research Institute through NASA Cooperative Agreement NCC 9-58, US Army Medical Research, and NYSTAR. The authors wish to thank Minyi Hu and Maria Magdalena Pritz for their excellent technical assistance on this paper.

References

1. Rubin C, Judex S, Qin YX. Low-level mechanical signals and their potential as a non-pharmacological intervention for osteoporosis. Age Ageing. 2006; 35(Suppl 2):ii32–ii36. [PubMed: 16926201]
2. Rubin C, Turner AS, Bain S, Mallinckrodt C, McLeod K. Anabolism. Low mechanical signals strengthen long bones. Nature. 2001; 412:603–4. [PubMed: 11493908]
3. Garman R, Gaudette G, Donahue LR, Rubin C, Judex S. Low-level accelerations applied in the absence of weight bearing can enhance trabecular bone formation. J Orthop Res. 2007; 25:732–40. [PubMed: 17318899]
4. Garman R, Rubin C, Judex S. Small oscillatory accelerations, independent of matrix deformations, increase osteoblast activity and enhance bone morphology. PLoS ONE. 2007; 2:e653. [PubMed: 17653280]
5. Qin YX, Kaplan T, Saldanha A, Rubin C. Fluid pressure gradients, arising from oscillations in intramedullary pressure, is correlated with the formation of bone and inhibition of intracortical porosity. J Biomech. 2003; 36:1427–37. [PubMed: 14499292]

6. Qin YX, Rubin CT, McLeod KJ. Nonlinear dependence of loading intensity and cycle number in the maintenance of bone mass and morphology. J Orthop Res. 1998; 16:482–9. [PubMed: 9747791]
7. Pohl P, Antoneko YN, Rosenfeld E. Effects of ultrasound on the pH profiles in the unstirred layers near bilayer lipid membranes measured by microelectrodes. Biochim Biophys Ata. 1993; 1152:155–60.
8. Pohl P, Rosenfeld E, Millner R. Effects of ultrasound on the steady-state transmembrane pH grardient and th epermeability of acetic acid through bilayer lipid membranes. Biochim Biophys Ata. 1993; 1145:279–83.
9. Nolte PA, Klein-Nulend J, Albers GH. Low intensity ultrasound stimulates in vitro endochondral ossification. Calcif Tissue Int. 1999; 64:S62.
10. Nolte PA, Klein-Nulend J, Albers GH, Marti RK, Semeins CM, Goei SW, Burger EH. Low-intensity ultrasound stimulates endochondral ossification in vitro. J Orthop Res. 2001; 19:301–7. [PubMed: 11347705]
11. Doan N, Reher P, Meghji S, Harris M. In vitro effects of therapeutic ultrasound on cell proliferation, protein synthesis and cytokine production by human fibroblasts, osteoblasts and monocytes. J Oral Maxillofac Surg. 1999; 57:409–19. [PubMed: 10199493]
12. Reher P, Doan N, Bradnock B, Meghji S, Harris M. Therapeutic ultrasound for osteonecrosis: An in vitro comparison between 1MHz and 45 kHz machines. Eur J Cancer. 1998; 34:1962–1968. [PubMed: 10023323]
13. Saito M, Fujii K, Tanaka T, Soshi S. Effect of low- and high-intensity pulsed ultrasound on collagen post-translational modifications in MC3T3-E1 osteoblasts. Calcif Tissue Int. 2004; 75:384–95. [PubMed: 15592795]
14. Saito M, Soshi S, Tanaka T, Fujii K. Intensity-related differences in collagen post-translational modification in MC3T3-E1 osteoblasts after exposure to low- and high-intensity pulsed ultrasound. Bone. 2004; 35:644–55. [PubMed: 15336600]
15. Tang CH, Lu DY, Tan TW, Fu WM, Yang RS. Ultrasound induces hypoxia-inducible factor-1 activation and inducible nitric-oxide synthase expression through the integrin/integrin-linked kinase/Akt/mammalian target of rapamycin pathway in osteoblasts. J Biol Chem. 2007; 282:25406–15. [PubMed: 17588951]
16. Hou CH, Hou SM, Tang CH. Ultrasound increased BMP-2 expression via PI3K, Akt, c-Fos/c-Jun, and AP-1 pathways in cultured osteoblasts. J Cell Biochem. 2009; 106:7–15. [PubMed: 19009553]
17. Azuma Y, Ito M, Harada Y, Takagi H, Ohta T, Jingushi S. Low-intensity pulsed ultrasound accelerates rat femoral fracture healing by acting on the various cellular reactions in the fracture callus. J Bone Miner Res. 2001; 16:671–80. [PubMed: 11315994]
18. Rawool NM, Goldberg BB, Forsberg F, Winder AA, Hume E. Power Doppler assessment of vascular changes during fracture treatment with low-intensity ultrasound. J Ultrasound Med. 2003; 22:145–53. [PubMed: 12562119]
19. Pilla AA, Mont MA, Nasser PR, Khan SA, Figueiredo M, Kaufman JJ, Siffert RS. Non-invasive low-intensity pulsed ultrasound accelerates bone healing in the rabbit. J Orthop Trauma. 1990; 4:246–53. [PubMed: 2231120]
20. Wang SJ, Lewallen DG, Bolander ME, Chao EY, Ilstrup DM, Greenleaf JF. Low intensity ultrasound treatment increases strength in a rat femoral fracture model. J Orthop Res. 1994; 12:40–7. [PubMed: 8113941]
21. Yang KH, Parvizi J, Wang SJ, Lewallen DG, Kinnick RR, Greenleaf JF, Bolander ME. Exposure to low-intensity ultrasound increases aggrecan gene expression in a rat femur fracture model. J Orthop Res. 1996; 14:802–9. [PubMed: 8893775]
22. Cook SD, Ryaby JP, McCabe J, Frey JJ, Heckman JD, Kristiansen TK. Acceleration of tibia and distal radius fracture healing in patients who smoke. Clin Orthop Relat Res. 1997:198–207. [PubMed: 9137191]
23. Cook SD, Salkeld SL, Mse, Patron LP, Ryaby JP, Whitecloud TS. Low-intensity pulsed ultrasound improves spinal fusion. Spine J. 2001; 1:246–54. [PubMed: 14588328]
24. Heckman JD, Sarasohn-Kahn J. The economics of treating tibia fractures. The cost of delayed unions. Bull Hosp Jt Dis. 1997; 56:63–72. [PubMed: 9063607]

25. Leung KS, Lee WS, Tsui HF, Liu PP, Cheung WH. Complex tibial fracture outcomes following treatment with low-intensity pulsed ultrasound. Ultrasound Med Biol. 2004; 30:389–95. [PubMed: 15063521]
26. Yang RS, Chen YZ, Huang TH, Tang CH, Fu WM, Lu BY, Lin WL. The effects of low-intensity ultrasound on growing bone after sciatic neurectomy. Ultrasound Med Biol. 2005; 31:431–7. [PubMed: 15749567]
27. Warden SJ, Bennell KL, Forwood MR, McMeeken JM, Wark JD. Skeletal effects of low-intensity pulsed ultrasound on the ovariectomized rodent. Ultrasound Med Biol. 2001; 27:989–98. [PubMed: 11476933]
28. Warden SJ, Bennell KL, Matthews B, Brown DJ, McMeeken JM, Wark JD. Efficacy of low-intensity pulsed ultrasound in the prevention of osteoporosis following spinal cord injury. Bone. 2001; 29:431–6. [PubMed: 11704494]
29. Carvalho DC, Cliquet Junior A. The action of low-intensity pulsed ultrasound in bones of osteopenic rats. Artif Organs. 2004; 28:114–8. [PubMed: 14720297]
30. Spadaro JA, Albanese SA. Application of low-intensity ultrasound to growing bone in rats. Ultrasound Med Biol. 1998; 24:567–73. [PubMed: 9651966]
31. Fyhrie DP, Hoshaw SJ, Hamid MS, Hou FJ. Shear stress distribution in the trabeculae of human vertebral bone. Ann Biomed Eng. 2000; 28:1194–9. [PubMed: 11144980]
32. Ruimerman R, Van Rietbergen B, Hilbers P, Huiskes R. The effects of trabecular-bone loading variables on the surface signaling potential for bone remodeling and adaptation. Ann Biomed Eng. 2005; 33:71–8. [PubMed: 15709707]
33. Parfitt AM, Drezner MK, Glorieux FH, Kanis JA, Malluche H, Meunier PJ, Ott SM, Recker RR. Bone histomorphometry: standardization of nomenclature, symbols, and units. Report of the ASBMR Histomorphometry Nomenclature Committee. J Bone Miner Res. 1987; 2:595–610. [PubMed: 3455637]
34. Heybeli N, Yesildag A, Oyar O, Gulsoy UK, Tekinsoy MA, Mumcu EF. Diagnostic ultrasound treatment increases the bone fracture-healing rate in an internally fixed rat femoral osteotomy model. J Ultrasound Med. 2002; 21:1357–63. [PubMed: 12494977]
35. NEMA, N. Revision3 NEMA UD 2–2004. 2004. Acoustic Output Measurement Standard for Diagnostic Ultrasound Equipment.
36. Duarte LR. The stimulation of bone growth by ultrasound. Arch Orthop Trauma Surg. 1983; 101:153–9. [PubMed: 6870502]
37. Chang WH, Sun JS, Chang SP, Lin JC. Study of thermal effects of ultrasound stimulation on fracture healing. Bioelectromagnetics. 2002; 23:256–63. [PubMed: 11948604]
38. Lim D, Ko CY, Seo DH, Woo DG, Kim JM, Chun KJ, Kim HS. Low-intensity ultrasound stimulation prevents osteoporotic bone loss in young adult ovariectomized mice. J Orthop Res. 2011; 29(1):116–25. [PubMed: 20607839]
39. Yang KH, Park SJ. Stimulation of fracture healing in a canine ulna full-defect model by low-intensity pulsed ultrasound. Yonsei Med J. 2001; 42:503–8. [PubMed: 11675678]
40. Pilla AA. Low-intensity electromagnetic and mechanical modulation of bone growth and repair: are they equivalent? J Orthop Sci. 2002; 7:420–8. [PubMed: 12077675]
41. Montalibet A, Jossinet J, Matias A, Cathignol D. Electric current generated by ultrasonically induced Lorentz force in biological media. Med Biol Eng Comput. 2001; 39:15–20. [PubMed: 11214267]
42. Nahirnyak V, Mast TD, Holland CK. Ultrasound-induced thermal elevation in clotted blood and cranial bone. Ultrasound Med Biol. 2007; 33:1285–95. [PubMed: 17490808]
43. Duck FA. Hazards, risks and safety of diagnostic ultrasound. Med Eng Phys. 2008; 30:1338–48. [PubMed: 18635388]
44. Chen H, Li X, Wan M. Spatial-temporal dynamics of cavitation bubble clouds in 1.2 MHz focused ultrasound field. Ultrason Sonochem. 2006; 13:480–6. [PubMed: 16571378]
45. Han Y, Cowin SC, Schaffler MB, Weinbaum S. Mechanotransduction and strain amplification in osteocyte cell processes. Proc Natl Acad Sci U S A. 2004; 101:16689–94. [PubMed: 15539460]
46. Weinbaum S, Guo P, You L. A new view of mechanotransduction and strain amplification in cells with microvilli and cell processes. Biorheology. 2001; 38:119–42. [PubMed: 11381170]

47. Warden S, Bennell K, McMeeken J, Wark J. Can conventional therapeutic ultrasound units be used to accelerate fracture repair? Phys Ther Rev. 1999; 4:117–126.

48. Nicholson PH, Muller R, Cheng XG, Ruegsegger P, Van Der Perre G, Dequeker J, Boonen S. Quantitative ultrasound and trabecular architecture in the human calcaneus. J Bone Miner Res. 2001; 16:1886–92. [PubMed: 11585354]

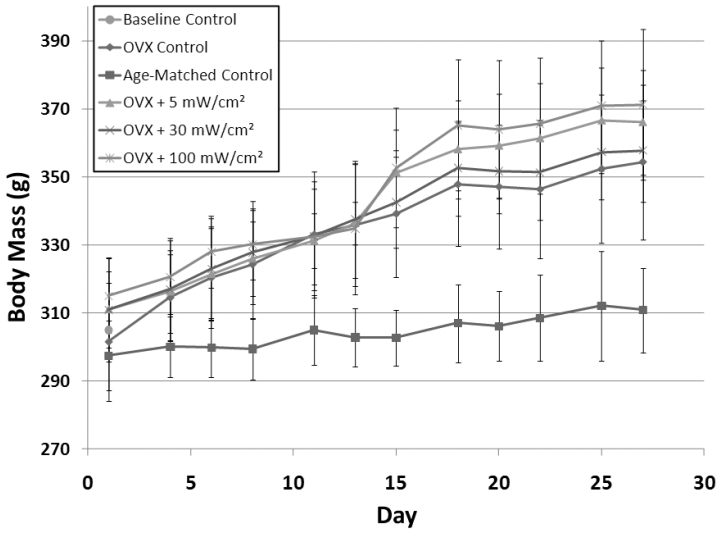

Figure 1.
Body mass in grams for experimental and control groups throughout the 28 day experiment.

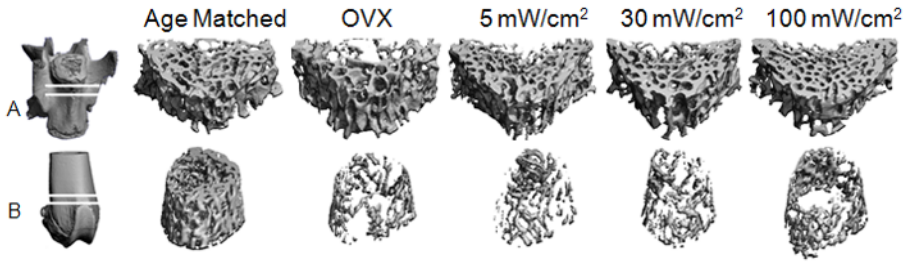

Figure 2.
Representative μCT images of cancellous bone in the L5 vertebra (A) and distal femoral metaphysis (B) for experimental and control groups.

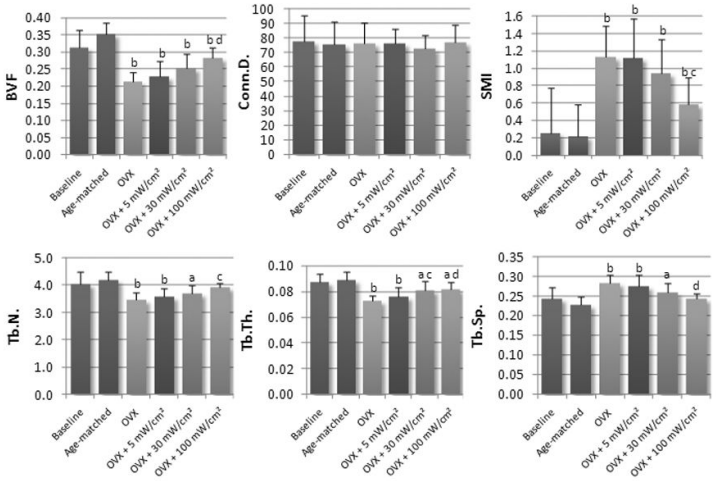

Figure 3.

Mean values of microstructural parameters at the L5 vertebra for experimental and control groups. Values are reported as mean ± SD. (Note: a = $p<0.05$ vs. age-matched control, b = $p<0.001$ vs. age-matched control, c = $p<0.05$ vs. OVX control, d = $p<0.001$ vs. OVX control.)

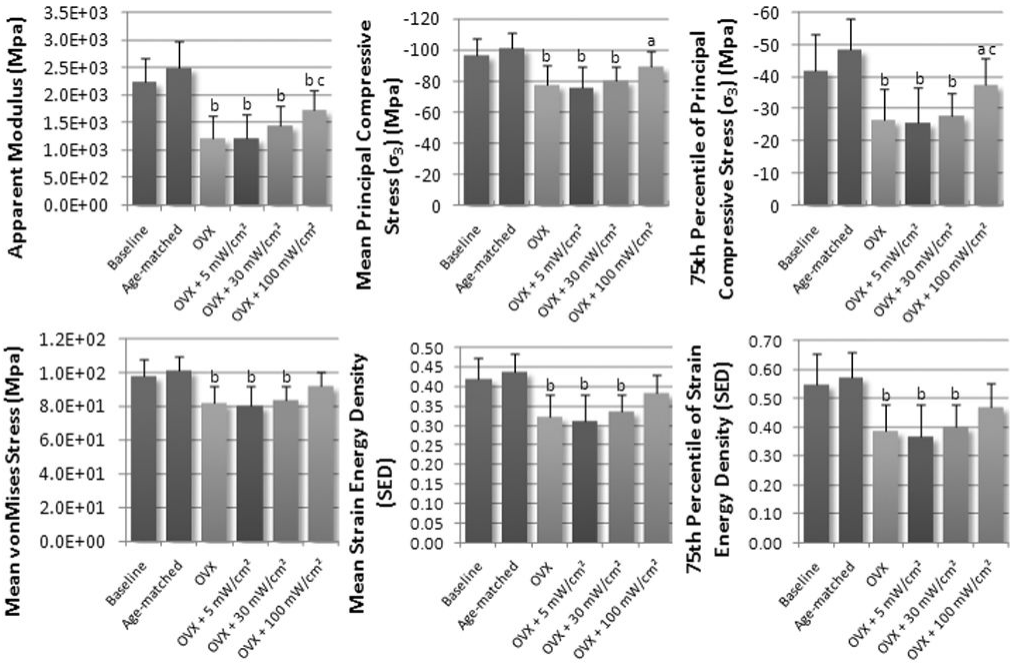

Figure 4.

Mean values of strength parameters at the L5 vertebra for experimental and control groups. Values are reported as mean ± SD. (Note: a = $p<0.05$ vs. age-matched control, b = $p<0.001$ vs. age-matched control, c = $p<0.05$ vs. OVX control, d = $p<0.001$ vs. OVX control.)

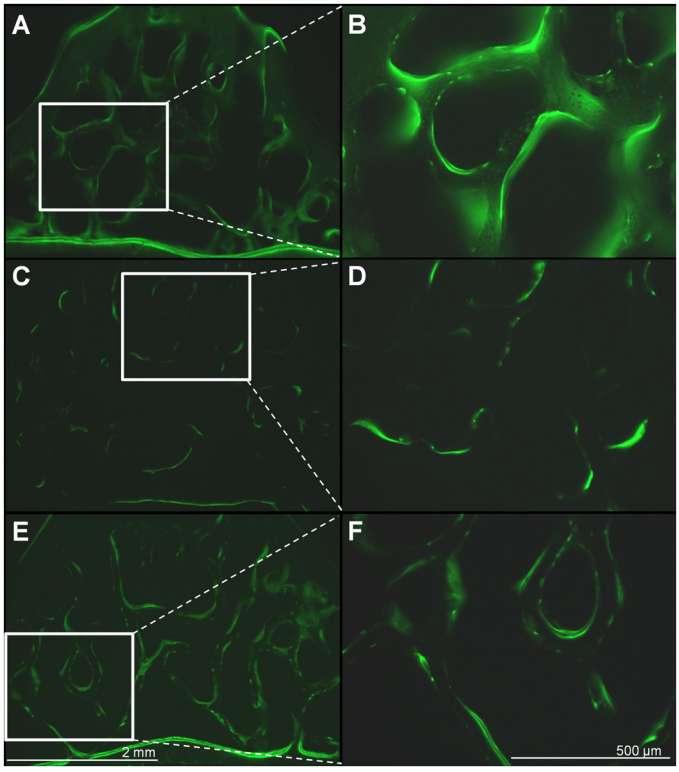

Figure 5.
Representative fluorescent images of calcein labeled transverse vertebral slices for Age-matched controls (A,B), OVX controls (C,D) and OVX + 100mW/cm^2 US treated animals(E,F). Images on the left are taken at 4× magnification and images on the right depict the 10× view of regions indicated by the white box at the left. Scale bars for 4× and 10× images are shown in E and F.

Table 1

Percent difference in trabecular microstructure parameters for the L5 vertebral body for experimental and control groups.

	BV/TV	Conn.D.	SMI	Tb.N.	Tb.Th.	Tb.Sp.
OVX vs. Age-matched	−40% ††	1%	436% ††	−17% ††	−19% ††	24% ††
OVX + 5 mW/cm^2 vs. OVX	8%	−1%	−1%	3%	5%	−2%
OVX + 30 mW/cm^2 vs. OVX	19%	−4%	−17%	7%	11% *	−8%
OVX + 100 mW/cm^2 vs. OVX	33% **	1%	−48% *	12% *	13% **	−14% **
OVX + 5 mW/cm^2 vs. Age-matched	−35% ††	1%	432% ††	−15% ††	−14% ††	21% ††
OVX + 30 mW/cm^2 vs. Age-matched	−28% ††	−3%	347% ††	−11% †	−10%	15% ††
OVX + 100 mW/cm^2 vs. Age-matched	−20% ††	3%	177% ††	−7%	−8% ††	7%

Statistical significance is noted as follows:

† p<0.05 vs. Age-matched Control,

†† p<0.001 vs. Age-matched Control

* p<0.05 vs. OVX Control,

** p<0.002 vs. OVX Control.

Table 2

Percent difference in trabecular mechanical strength parameters for the L5 vertebral body for experimental and control groups.

	Apparent Elastic Modulus	Average *von*Mises Stress	Coefficient of Variation of *von*Mises Stress	Average Maximum Principal Compressive Stress	75th Percentile of Maximum Principal Compressive Stress	Average Strain Energy Density	75th Percentile of Strain Energy Density
OVX vs. Age-matched	−51% ††	−19% ††	21% ††	−23% ††	−45% ††	−26% ††	−32% ††
OVX + 5 mW/cm^2 vs. OVX	−1%	−2%	1%	−3%	−2%	−3%	−5%
OVX + 30 mW/cm^2 vs. OVX	18%	3%	−2%	3%	6%	4%	3%
OVX + 100 mW/cm^2 vs. OVX	42% *	13%	−10%	15%	41% *	18%	21%
OVX + 5 mW/cm^2 vs. Age-matched	−52% ††	−21% ††	22% ††	−25% ††	−46% ††	−29% ††	−36% ††
OVX + 30 mW/cm^2 vs. Age-matched	−42% ††	−18% ††	21% ††	−21% ††	−42% ††	−23% ††	−30% ††
OVX + 100 mW/cm^2 vs. Age-matched	−31% ††	−9%	9%	−11% †	−22% †	−13%	−18%

Statistical significance is noted as follows:

† p<0.05 vs. Age-matched Control,

†† p<0.001 vs. Age-matched Control

* p<0.05 vs. OVX Control,

** p<0.002 vs. OVX Control.

Table 3

L5 Vertebral Histomorphometry. Values are reported as mean ± SD; BV/TV is histomorphometric bone volume fraction, MS/BS is mineralized surface/bone surface; MAR is mineral apposition rate; BFR/BS is bone formation rate/bone surface.

	Age-Matched	OVX	OVX+5 mW/cm^2	OVX+30 mW/cm^2	OVX+100 mW/cm^2
BV/TV	29.61 ± 3.39 **	16.01 ± 1.50 ††	18.48 ± 2.11 ††	19.16 ± 2.53 ††	24.35 ± 4.11 ** ††
MS/BS (%)	16.08 ± 3.12 **	10.83 ± 2.15 ††	11.05 ± 1.65 ††	12.20 ± 2.41 †	14.15 ± 1.77 *
MAR (μm/day)0.69	0.69 ± 0.14 **	0.52 ± 0.10 ††	0.52 ± 0.05 †	0.61 ± 0.10	0.63 ± 0.14
BFR/BS (μm^3/μm^2/yr)	42.10 ± 0.04 **	19.38 ± 0.02 ††	21.01 ± 0.01 ††	28.00 ± 0.03 †	30.85 ± 0.01

Note:

† p<0.05 vs. Age-matched Control,

†† p<0.001 vs. Age-matched Control

* p<0.05 vs. OVX Control,

** p<0.002 vs. OVX Control